Contrib Mineral Petrol (2001) 142: 244–259
DOI 10.1007/s004100100289

M. Grégoire · I. Jackson · S.Y. O'Reilly · J.Y. Cottin

The lithospheric mantle beneath the Kerguelen Islands (Indian Ocean): petrological and petrophysical characteristics of mantle mafic rock types and correlation with seismic profiles

Received: 14 August 2000 / Accepted: 22 May 2001 / Published online: 21 July 2001

Abstract Deep-seated meta-igneous xenoliths brought to the surface by alkali basaltic magmas from the Kerguelen Islands reveal that basaltic magmas have intruded the upper mantle throughout their geological evolution. These xenoliths record volcanic activity associated with their early South East Indian Ridge location and subsequent translation to an intraplate setting over the Kerguelen Plume. The meta-igneous xenoliths sample two distinctive geochemical episodes: one is tholeiitic transitional and one is alkali basaltic. Geothermobarometry calculations provide a spatial context for the rock type sequence sampled and for interpreting petrophysical data. The garnet granulites equilibrated over a pressure range of 1.15 to 1.35 GPa and the garnet pyroxenite at 1.8 GPa. Ultrasonic measurements of compressional wave speed V_P have been carried out at pressures up to 1 GPa, and densities measured for representative samples of meta-igneous xenoliths and for a harzburgite that represents the peridotitic mantle. V_P and density have also been calculated using modal proportions of minerals and appropriate elastic properties for the constituent minerals. Calculated and measured V_P agree well for rock types with microstructures not complicated by kelyphitic breakdown of garnet and/or pervasive grain-boundary cracking. Pyroxene granulites have measured and calculated V_P within the range 7.37–7.52 km/s; calculated velocities for the garnet granulites and pyroxenites range from 7.69 to 7.99 km/s, whereas measured and calculated V_P for a mantle harzburgite are 8.45 and 8.29 km/s respectively. The seismic structure observed beneath the Kerguelen Islands can be explained by (1) a mixture of underplated pyroxene granulites and ultramafic rocks responsible for the 2–3 km low velocity transitional zone below the oceanic layer 3, (2) varying proportions of granulites and pyroxenites in different regions within the upper mantle producing the lateral heterogeneities, and (3) intercalation of the granulites and pyroxenites throughout the entire upper mantle column, along with elevated temperatures, accounting for the relatively low mantle velocities (7.70–7.95 km/s).

M. Grégoire (✉) · S.Y. O'Reilly
GEMOC ARC National Key Centre,
Department of Earth and Planetary Sciences,
Macquarie University, NSW 2109, Australia
E-mail: mgregoire@geology.uct.ac.za

I. Jackson
Research School of Earth Sciences,
Australian National University,
Canberra, ACT 0200, Australia

J.Y. Cottin
Department of Geology-UMR 6524,
University J. Monnet, 23 rue P. Michelon,
42023 St-Etienne, France

Present address: M. Grégoire
Department of Geological Sciences,
University of Cape Town, Rondebosch,
7701 South Africa
Tel.: +27-21-6502909, Fax: +27-21-6503783

Editorial responsibility: J. Hoefs

Introduction

Ultramafic and mafic xenoliths provide unique and direct information about the nature, composition, structure and evolution of the lower crust, upper mantle and crust–mantle transition zone (e.g. Frey and Prinz 1978; Griffin et al. 1984; O'Reilly and Griffin 1987; O'Reilly et al. 1990; Grégoire et al. 1998). Seismic profiles give indirect information on the properties of the lower crustal and upper mantle rocks in situ (e.g. Finlayson and Leven 1987; Recq et al. 1990). Laboratory measurement of the petrophysical parameters, compressional wave velocity (V_P) and density (ρ) of the xenoliths allows comparison between these different sources of information on the deep part of the lithosphere and provides constraints for the interpretation of the seismic data in a geologically meaningful way (e.g. O'Reilly et al. 1990; Rudnick and Fountain 1995; Rudnick and Jackson 1995).

Seismic refraction studies (Recq et al. 1990, 1994; Charvis et al. 1995) show evidence for thickened oceanic crust in the Kerguelen archipelago. They indicate that the oceanic layer 2 (Vp: 4.6–4.8 km/s) is 8 to 9 km thick with oceanic layer 3 (V_P: 6.6–7.0 km/s) about 5 to 10 km thick and extending from a depth of about 10 km to a base at 15–20 km in different parts of the seismic profiles. Beneath layer 3, there is a seismically distinct zone 2–3 km thick that shows a range in V_P increasing from about 7.2 to 7.5 km/s with depth; these values are significantly lower than the usual V_P at this depth in the oceanic lithosphere. This zone has been interpreted as a transitional zone representing a layered crust–mantle boundary (e.g. Recq et al. 1990; Grégoire et al. 1998).

The seismic refraction data (Recq et al. 1990; Charvis et al. 1995) also show that the P-wave velocities within the upper mantle are relatively low (7.70–7.95 km/s) and that there are lateral variations in V_P within the lower crust and the upper mantle. These have been interpreted previously as lithological heterogeneities due to the presence of serpentinised mantle peridotite regions or to magmatic underplating processes.

Grégoire et al. (1998) identified the role of deep-seated magmatic additions to the lithosphere beneath Kerguelen as an important part of crustal growth in this region and a possible mechanism of continental nucleation. This study builds on that petrological work and focuses on interpreting the new petrophysical (V_P, ρ) data using petrological and geochemical (major and trace element) information for both bulk rocks and constituent minerals for a representative subset of the meta-igneous xenoliths [termed Type II in accordance with the terminology of Frey and Prinz (1978)] from the lithospheric mantle beneath the Kerguelen Islands. The xenoliths are frozen basaltic melts and cumulates intruded into the upper mantle and subsequently equilibrated to the temperature and pressure conditions of granulite facies. They represent crystallisation products from the magmas produced in multiple melting episodes beneath the Kerguelen plateau (Weis et al. 1993; Yang et al. 1998) and record the intrusion of successive sills and lenses of basaltic melts spanning the long and complex volcanic history of this region (Grégoire et al. 1998). These xenoliths provide geochemical evidence to distinguish the different contributions of magmatism associated with both mid-ocean ridge and plume activity. Their formation is therefore an integral part of the geological evolution of the archipelago and especially reflects the vigorous activity of the Kerguelen mantle plume. Because we can put these rock types into a spatial context using geothermobarometry, we can assess the nature of construction and the architecture of the plateau at depths from about 10 to 50 km (sampled by the xenoliths), and integrate the geological data from these xenoliths with their petrophysical characteristics to provide realistic constraints to interpret the deep geophysical (mainly seismic) data for the Kerguelen Islands. The Type I

Table 1 Locality and paragenesis of the Kerguelen Type II xenoliths (*numbers after localities* refer to Fig. 1)

Sample no.	OB93-57	GM92-412	GM92-347	GM92-394	GM92-390	GM92-165	GM92-453
Rock type	Two-pyroxene granulites		Garnet two-pyroxene granulites			Garnet pyroxenite	Spinel harzburgite
Affinity	Tholeiitic–transitional (metamorphosed cumulates)		Tholeiitic–transitional (metamorphosed cumulates or frozen melts)			Alkali basaltic cumulate	Mantle peridotite
			Cumulate	Intermediate	Frozen melt		
Xen. type	Type IIa	Type IIa	Type IIa	Type IIa/IIc	Type IIc	Type IIb	Type I
Assemblage	cpx–opx–pl–sp	cpx–opx–pl–sp–sapph	cpx–opx–pl–sp–ga–sapph	cpx–opx–pl–sp–ga–ru	cpx–opx–pl–ga–ilm–am	cpx–opx–pl–sp–ga–ilm	ol–opx–cpx–sp
Locality	Val Studer, 4	Mt. Tizzard, 1	Mt. Tizzard, 1	Mt. Tizzard, 1	Mt. Tizzard, 1	Val Phonolite, 2	Le triedre, 3

xenolith, a harzburgite (sample GM92-453, described in detail in Grégoire et al. 2000) was included in this study in order to assess the petrophysical characteristics of the peridotitic upper mantle wall-rock beneath the Kerguelen archipelago. Previous studies (e.g. Grégoire et al. 1997, 2000) have detailed the petrology and composition of the Kerguelen peridotitic upper mantle.

Geological setting

The Kerguelen Islands are located in the oceanic domain of the Antarctic plate and represent the thickest section of the Kerguelen oceanic plateau, which is the second largest oceanic plateau (25×106 km^3) after the Ontong Java plateau (Coffin and Eldhom 1993). The Kerguelen Islands have evolved from a location near the SEIR (South East Indian Ridge) to a present-day intraplate setting and the magmatic activity has extended over 45 m.y. (e.g. Giret 1993). Their geodynamic evolution records a progressive change in composition of basaltic magmas from tholeiitic to alkaline (Gautier et al. 1990; Weis et al. 1993). Therefore, the Kerguelen Islands present a unique geological setting combining characteristics of both the Iceland and Hawaiian regions (Giret et al. 1997). This is an unusual oceanic tectonic environment (and possibly analogous to that of the smaller Agulhas plateau; Uenzelmann-Neben et al. 1999; Gohl and Uenzelmann-Neben 2001) but it may be relevant to an important mechanism for the nucleation and growth of continental nuclei (Grégoire et al. 1995, 1998).

Ultramafic and mafic xenoliths from the Kerguelen Islands occur in dykes, lava-flows and breccia pipes of the youngest and more alkaline basaltic rocks (Grégoire et al. 1994, 1997, 1998). The mantle and meta-igneous xenoliths studied here were collected from four different localities of the Kerguelen archipelago (Fig. 1 and Table 1). They have sub-rounded shapes and range from 10 to 30 cm in diameter. They correspond to Type I and Type II Kerguelen xenoliths defined by Grégoire et al. (1997, 1998, 2000).

Sampling and analytical methods

Six xenoliths large enough for laboratory determination of acoustic velocity were chosen to represent the different types of meta-igneous xenoliths identified from Kerguelen.

Samples were taken from the central parts of the xenoliths and ground in an agate mill. Major and minor elements (Cr, Ni) in bulk rocks were analysed by X-ray fluorescence spectrometry (XRF) at Macquarie University (see O'Reilly and Griffin 1988 for methods). The concentration of 30 minor and trace elements in bulk rocks (REE, Ba, Cs, Rb, Th, U, Nb, Ta, Pb, Sr, Zr, Ti, Y, Sc, V, Co, Cu and Zn) were analysed using a Perkin-Elmer Sciex ELAN 6000 ICP-MS instrument at Macquarie University. Mineral major and minor element compositions were determined by a Cameca Camebax SX 50 microprobe at Macquarie University using a wavelength-dispersive spectrometric (WDS) technique. The microprobe was used with 15 kV accelerating voltage, sample current of 20 nA, a beam diameter of 2–3 μm, and natural and synthetic minerals as standards. Count times were 20–40 s and no values are reported below detection limits (0.01–0.04 wt%).

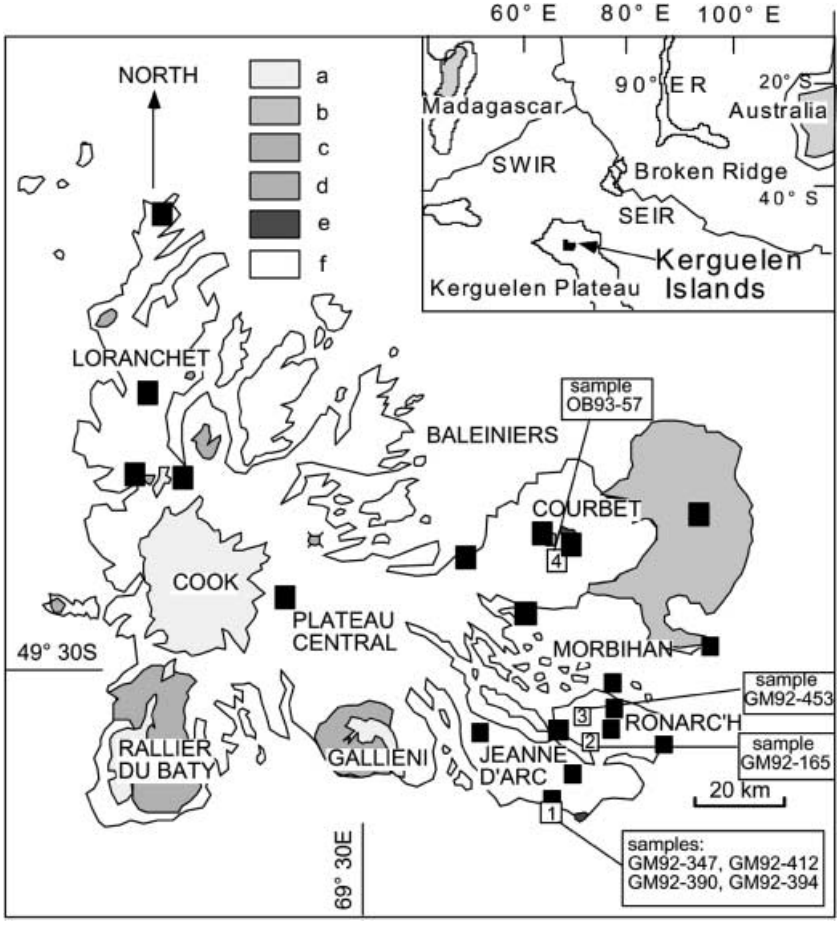

Fig. 1 Location of ultramafic and mafic xenolith-bearing alkali basalts of the Kerguelen Islands (modified after Grégoire et al. 1997, 2000). *a* Ice caps; *b* moraines; *c* alkaline silica-oversaturated volcano-plutonic complexes; *d* alkaline silica-undersaturated volcano-plutonic complexes; *e* tholeiitic–transitional plutonic complexes; *f* flood basalts of transitional to alkaline type. Ultramafic and mafic xenolith-outcrops shown as *solid squares*; *numbered open squares* refer to sample locality (see Table 1 for the naming of each outcrop). *Inset* shows location of Kerguelen Islands, South West Indian Ridge (*SWIR*) and the South East Indian Ridge (*SEIR*)

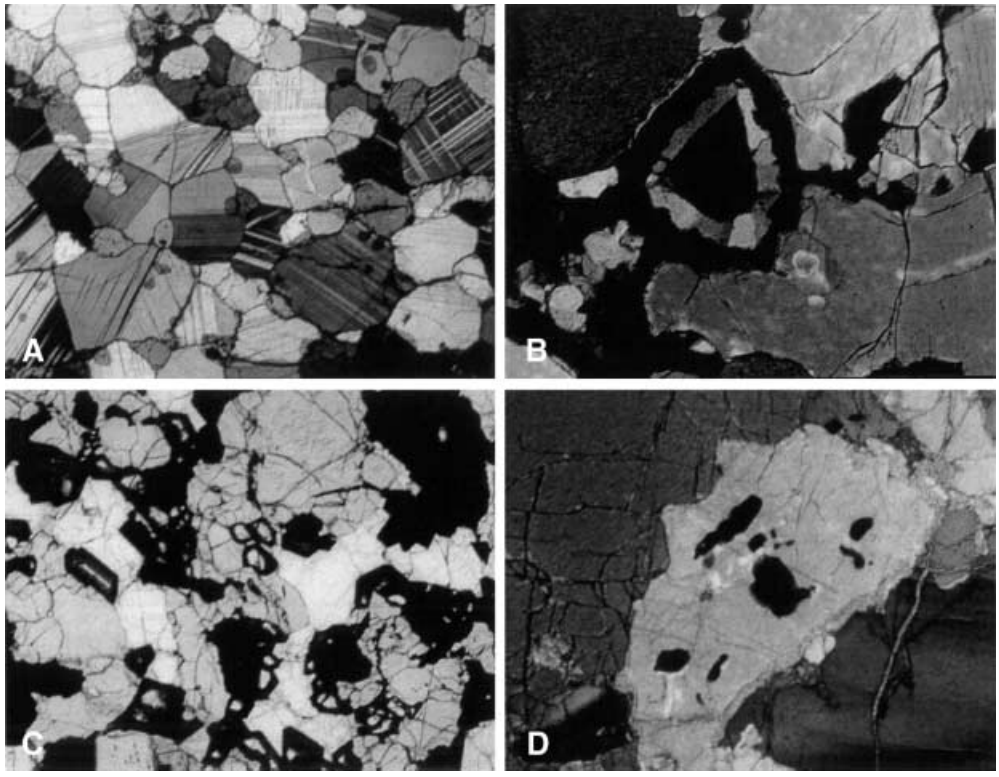

Fig. 2 Photomicrographs of the Kerguelen xenoliths. **A** Granoblastic-mosaic texture (sample 0B93-57, ×25). **B** Garnet and sapphirine coronites around spinel (sample GM92-347, ×50). **C** Garnet granulites of Type IIc (sample GM92-390) showing significant replacement of garnet by kelyphite (×25). **D** Poikilitic spinel-bearing harzburgite (sample GM92-453). Clinopyroxene encloses spinel grains (×50)

Petrography

The samples studied here in detail are all Type II (Frey and Prinz 1978) and comprise two-pyroxene granulites (samples GM92-412 and OB93-57), garnet granulites (samples GM92-347, GM92-390 and GM92-394) and a garnet pyroxenite (GM92-165), as summarised in Table 1. The xenoliths can be grouped into two main geochemical types as detailed in Grégoire et al. (1998).

The first group has basaltic tholeiitic–transitional characteristics and includes Type IIa (e.g. samples GM92-412, OB93-57, GM92-347), which are cumulates and Type IIc (e.g. sample GM92-390), which are frozen melts (Grégoire et al. 1998). Sample GM92-394 shows petrographic characteristics that are intermediate between those of Type IIa and Type IIc and is designated IIa/IIc.

The second group has alkali basaltic affinities and is represented by the garnet clinopyroxenite (sample GM92-165) and designated Type IIb (Grégoire et al. 1998).

The main microstructures of Type II xenoliths are allotriomorphic–granular heterogranular, but some are hypidiomorphic–granular. All the samples show local recrystallisation to granoblastic-mosaic textures (Fig. 2). Most of the granulite samples (GM92-412, GM92-347, GM92-390 and GM92-394) have evidence of subsolidus re-equilibration characterised by the widespread development of coronitic and symplectitic mineral parageneses. The coronitic and symplectitic minerals at the grain boundaries between pyroxenes, spinel and plagioclase are garnet + clinopyroxene2 in samples GM92-390 and 394, garnet + clinopyroxene2 + sapphirine in sample GM92-347 and clinopyroxene2 + sapphirine in sample GM92-412 (Grégoire et al. 1994, 1998). The garnet and sapphirine coronites and symplectites are especially abundant in sample GM92-347 (Fig. 2). The rare secondary amphiboles occurring in the Type IIb and IIc xenoliths are derived by metasomatic reaction of pre-existing clinopyroxenes.

The grain size in the Type II xenoliths commonly ranges from 0.1 to 2–3 mm but goes up to 5 mm in clinopyroxenite GM92-165. Two garnet-bearing granulites (GM92-390 and 394; Fig. 2) show significant replacement of garnet by kelyphite (20 to 80% from one garnet to another), similar to that described by Griffin et al. (1987) and Rudnick and Jackson (1995) for the garnet granulite xenoliths from the Central and Chudleigh volcanic provinces of north Queensland (Australia). The clinopyroxenite GM92-165 displays a large amount of grain boundary alteration and hematite staining.

The Type I harzburgite chosen for this study (sample GM92-453) is a poikilitic harzburgite consisting of olivine (84 wt%), opx (13 wt%), cpx (2 wt%) and spinel (1 wt%). The poikilitic microstructure is similar to that described in some harzburgitic xenoliths from the French Massif Central (Coisy and Nicolas 1978) and is characterised by the occurrence of large olivine grains (up to 5 cm) enclosing orthopyroxene inclusions and by the habit of clinopyroxene (Fig. 2), which encloses olivine, orthopyroxene and spinel crystals (Grégoire et al. 1997, 2000).

Table 2 Bulk rock major (wt%) and trace element (ppm) abundances and calculated modal compositions of Type II xenoliths from the Kerguelen Islands

Sample	Type IIa GM92-412	Type IIa OB93-57	Type IIa GM92-347	Type IIa/IIc GM92-394	Type IIb GM92-165	Type IIc GM92-390
SiO_2	44.9	49.3	44.8	49.1	46.2	45.3
TiO_2	0.06	0.35	0.04	0.83	1.95	2.26
Al_2O_3	25.66	16.95	23.35	16.80	10.46	14.25
FeO	3.96	5.81	5.25	6.71	9.23	12.91
MnO	0.05	0.10	0.07	0.12	0.16	0.24
MgO	10.31	10.33	13.30	11.10	12.42	8.41
CaO	13.16	14.48	11.85	11.57	16.91	12.58
Na_2O	1.45	1.85	1.06	2.69	1.65	2.42
K_2O	0.08	0.05	0.07	0.16	0.12	0.14
P_2O_5	0.02	0.02	0.02	0.04	0.04	0.05
H_2O+	0.37	0.62	0.57	1.31	0.69	1.13
H_2O-	0.15	0.12	0.16	0.31	0.06	0.25
CO_2	0.07	0.13	0.03	0.05	0.11	0.20
Sum	100.3	100.1	100.5	100.7	100.0	100.1
Mg number	82.27	76.03	81.88	74.66	70.57	53.74
Sc	4.15	40.1	4.30	36.3	52.3	49.8
V	22.6	185	9.8	250	375	400
Cr (XRF)	730	480	505	840	270	300
Co	43	43	52	42	47	52
Ni (XRF)	300	170	430	250	135	90
Cu	15.0	4.00	5.95	21.7	26.6	56.6
Zn	15.5	30.8	21.3	35	56	160
Rb	1.47	0.49	2.77	5.32	3.70	6.79
Ba	26.6	10.7	17.4	47.4	18.0	21.5
Sr	274	164	156	224	120	149
Pb	0.100	0.131	0.220	0.231	0.770	0.307
Th	0.016	0.020	0.057	0.176	1.64	0.053
U	0.003	0.003	0.032	0.101	0.640	0.024
Nb	0.114	0.103	0.514	1.50	5.09	2.04
Ta	0.007	0.014	0.038	0.094	0.370	0.146
Ti	521	2200	308	4900	12500	12100
Zr	1.65	7.01	2.15	17.4	81	42
La	0.47	0.52	0.86	2.05	7.4	1.32
Ce	0.830	1.57	1.528	4.68	18.9	5.6
Pr	0.122	0.294	0.187	0.651	3.13	1.34
Nd	0.57	1.71	0.71	3.46	16.3	8.5
Sm	0.15	0.72	0.14	1.41	5.0	3.32
Eu	0.145	0.424	0.158	0.719	1.750	1.239
Gd	0.18	0.96	0.14	2.0	5.5	4.2
Dy	0.174	1.178	0.133	2.325	4.920	4.948
Ho	0.037	0.255	0.028	0.496	0.960	1.049
Er	0.11	0.70	0.08	1.37	2.45	2.97
Yb	0.09	0.62	0.08	1.17	1.86	2.54
Lu	0.01	0.09	0.01	0.17	0.25	0.37
Y	1.18	6.93	0.83	13.5	26.7	28.3

Major and trace element compositions

Whole rock composition

Major elements and transition trace elements (TTE)

All of the studied Type II xenoliths have mafic compositions, with SiO_2 ranging from 44.7 to 49.3 wt% and MgO contents varying from 8.4 to 13.3 wt% (Table 2). The Types IIb (alkaline) and IIc (tholeiitic–transitional melt) xenoliths are higher in TiO_2 than the Type IIa (tholeiitic–transitional cumulate) xenoliths. Sample GM92-394 (IIa/IIc) has an intermediate TiO_2 content (Table 2).

The two sapphirine-bearing Type IIa granulite xenoliths (GM92-412 and GM92-347) have high mg numbers and Al_2O_3 contents and extend the Mafic 1 field defined by Kempton and Harmon (1992) for granulite xenoliths worldwide to lower SiO_2/Al_2O_3 values (Fig. 3). Three other Kerguelen xenoliths (Type IIa granulite OB93-57, Type IIa/IIc granulite GM92-394 and Type IIb clinopyroxenite GM92-165) overlap the field of Mafic 1 granulites, but the Type IIc sample (GM92-390) plots in the 'primitive' basaltic magma field (Fig. 3). The Type IIa granulites and the intermediate IIa/IIc sample (GM92-394) have higher Cr (480–840 ppm) and Ni (170–430 ppm) contents than the Type IIb clinopyroxenite (Cr 272 ppm and Ni 135 ppm) and

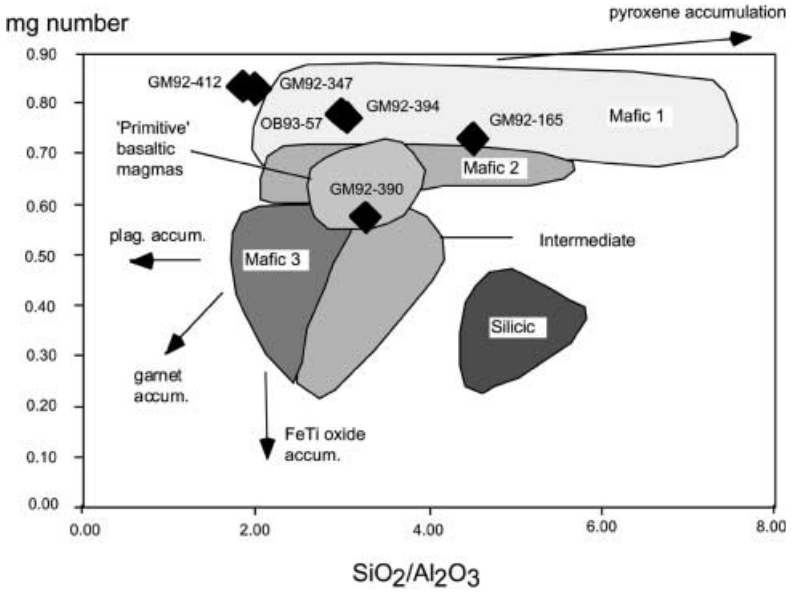

Fig. 3 Mg number vs. SiO_2/Al_2O_3 diagram for Kerguelen granulite and pyroxenite xenoliths compared with fields for granulite xenoliths worldwide. Definition of fields from Kempton and Harmon (1992). *Mafic 1* mafic granulites (i.e. $SiO_2 < 54$ wt%, mg number < 0.6; *intermediate* $SiO_2 > 54$ wt% and < 66 wt%; *silicic* $SiO_2 > 66$ wt%. Note that, for this diagram only, mg number is defined as $Mg/(Mg + 0.85\ FeO_{tot})$, to be consistent with Kempton and Harmon (1992). *Unbroken arrows* show generalised direction of compositional change with accumulation of indicated mineral phase

the Type IIc granulite (Cr 302 ppm and Ni 91 ppm) but lower Cu, Zn, Sc and V contents (Table 2). The Type IIa granulite GM92-347 is especially low in Sc (4.30 ppm) and V (9.80 ppm) and high in Ni (430 ppm) in comparison to the other samples (Table 2).

Other trace elements (REE, Y, HFSE, LILE)

The Type IIa (tholeiitic–transitional cumulate) granulite xenoliths have low REE contents (less than three times primitive mantle values) and have consistent positive Eu anomalies, especially pronounced in the two sapphirine-bearing samples which are also characterised by a LREE/HREE ratio > 1 (Fig. 4). The Type IIb (alkaline) clinopyroxenite and the Type IIc (tholeiitic–transitional melt) granulite are higher in total REE than Type IIa (tholeiitic–transitional cumulate). Type IIb shows slight LREE enrichment while Type IIc is characterised by a flat pattern from Pr to Lu with depletion in La and Ce. The Type IIa/IIc sample (GM92-394) displays a similar REE pattern to those of the Type IIa sample OB93-57, but its REE content is higher, its positive Eu anomaly is smaller and it plots between the Type IIa and the Type IIc xenoliths (Fig. 4).

All the studied Type II xenoliths have negative Zr anomalies (Fig. 5). The high Sr content of the Type IIa and IIa/IIc granulites results in the large positive Sr anomalies in their incompatible trace element patterns (Fig. 5). These patterns have very similar shapes for the elements from Ce to Lu, but the two garnet-bearing rocks are higher in Th, U, Nb, Ta and La than the two garnet-free samples. The Type IIb clinopyroxenite trace element pattern is characterised by positive Th and U anomalies and negative Pb and Sr anomalies. The Type IIc granulite has negative Th, U, and Pb anomalies.

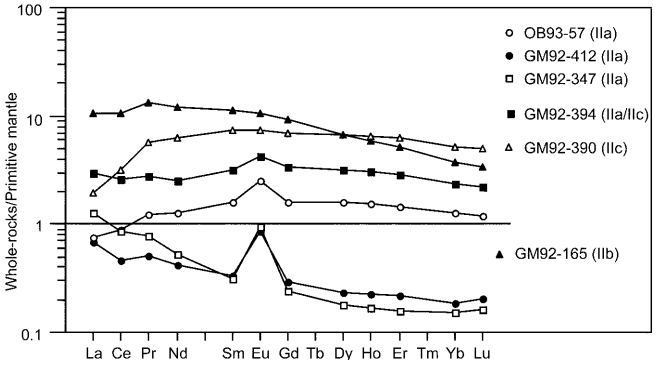

Fig. 4 Primitive mantle-normalised REE patterns for whole rock of Kerguelen granulite and pyroxenite xenoliths. Normalising values after McDonough and Sun (1995)

Mineral compositions

The clinopyroxenes of Type II xenoliths (Table 3) are aluminous diopsides (Al_2O_3: 6.65–7.80 wt%) poor in chromium ($Cr_2O_3 < 0.20$ wt%). Mg numbers [100 Mg/(Mg + Fe)] decrease from the Type IIa and IIa/IIc granulites (78.5–89.8) to Type IIb clinopyroxenite (73.8) and to the Type IIc granulite (69.2).

The orthopyroxene (Table 3) is an aluminous enstatite (Al_2O_3: 3.50–7.90 wt%). It shows a similar range in its mg number to those of the clinopyroxenes from Type IIa and IIa/IIc granulites (74.5–88.5) through to the Type IIb clinopyroxenite (73) and to the Type IIc granulite (70).

Plagioclase (Tables 3 and 4) is very high in CaO in the three Type IIa granulites (An 68–80; samples OB93-57, GM92-412 and GM92-347). The three other samples (GM92-165, GM92-390 and GM92-394) have more sodic plagioclase (An 34–42).

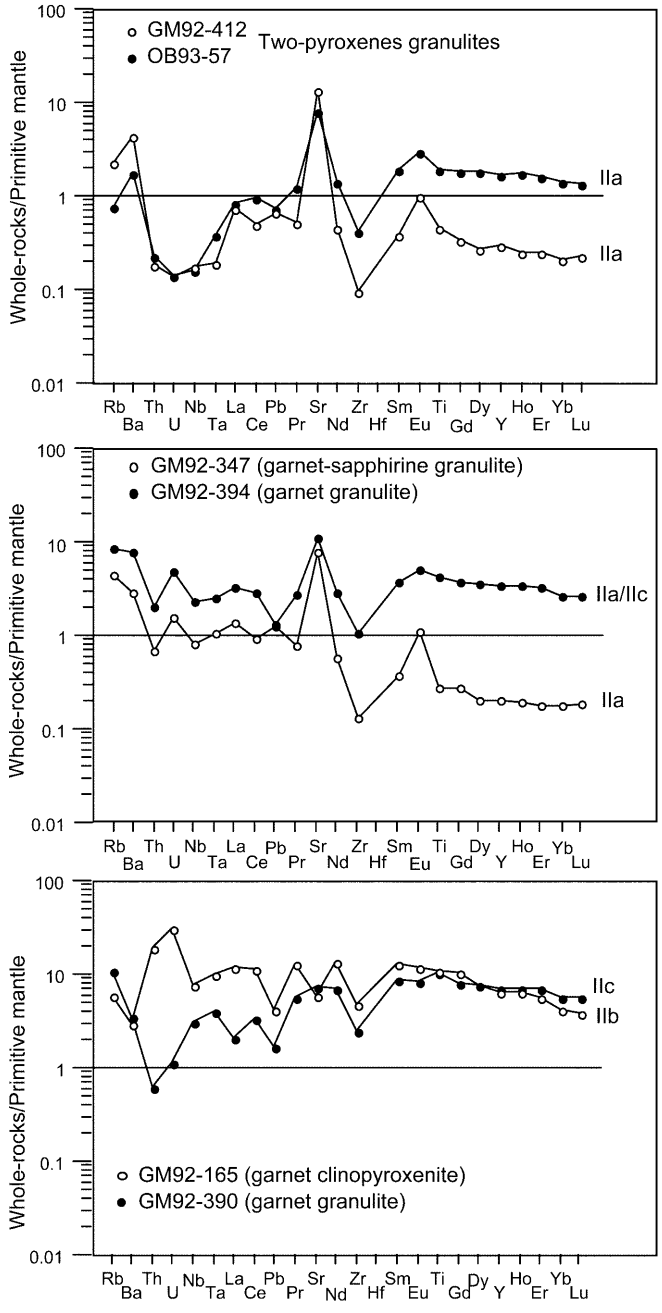

Fig. 5 Primitive mantle-normalised trace element patterns for whole rock from Kerguelen granulite and pyroxenite xenoliths. Normalising values after McDonough and Sun (1995)

The chemical composition of Type II Kerguelen garnets is controlled by Mg/Fe substitution, as shown by decreasing pyrope content with increasing almandine content from Type IIa sapphirine-bearing granulite to the Type IIa/IIc granulite, to Type IIb clinopyroxenite and to Type IIc granulite (Tables 3 and 4). The proportion of the grossular component does not vary.

Most Spinels are pleonastes (Table 3) with a low Cr_2O_3 content (mg number: 55–77.5 and cr number: 0.3–2.3). Type IIb and Type IIa/IIc spinels are higher in TiO_2 (0.4–0.45 wt%) than those of Type IIa (<0.10 wt%) (Table 3).

As already pointed out by Grégoire et al. (1998), ilmenite (Table 3) in the Type IIb clinopyroxenite is higher in TiO_2 (51.75 wt%) and MgO (4.5 wt%) than ilmenite in the Type IIc granulite (TiO_2: 41.15 wt% and MgO: 2.9 wt%).

Amphiboles (Table 3) of Type IIb and Type IIc xenoliths have similar mg numbers (63 and 63.35 respectively) but the Type IIb amphibole is slightly higher in TiO_2 (3.75 wt%), Al_2O_3 (14.5 wt%) and K_2O (0.95 wt%) than those of Type IIc (TiO_2: 3 wt%, Al_2O_3: 13.6 wt% and K_2O: 0.20 wt%).

Sapphirine (Table 3) in the garnet-bearing Type IIa granulite (GM92-347) is more magnesian (mg number: 89), higher in Al_2O_3 (62.70 wt%) and lower in SiO_2 (13.20 wt%) than its equivalent in garnet-free Type IIa granulite (GM92-412, mg number: 83; Al_2O_3: 59 wt% and SiO_2: 14.30 wt%).

Equilibration temperatures and pressures

Equilibration temperatures of the xenoliths studied were estimated using two-pyroxene geothermometers (Wells 1977; Brey and Köhler 1990) and clinopyroxene–garnet equilibria (Ellis and Green 1979) in the Kerguelen xenoliths. Equilibration pressures were estimated using orthopyroxene–garnet equilibria (Harley 1984). Core compositions of the primary large grains and FeO(total) have been used for the calculations. Our goal was to establish temperature and pressure ranges, using a consistent methodology, and these procedures are consistent with the protocols recommended in Xu et al. (1998). The chosen geothermometers and geobarometers are appropriate for the bulk compositions and relevant pressure and temperature ranges and have been shown by Xu et al. (1998) to give consistent results for the different bulk compositions of peridotites with adjacent pyroxenites or granulites in composite xenoliths. The results are given in Table 5. The two garnet-free granulitic samples, GM92-412 and OB93-57, give temperatures ranging from 800 to 900 °C and according to their mineral assemblages have been equilibrated in the 'pyroxene granulite stability field', i.e. within the pressure range from 0.5–0.8 to 1.1 GPa (Gasparik 1984; Wood and Holloway 1984 ; Grégoire et al. 1994, 1998). However, we can infer that these xenoliths equilibrated at the higher pressure end of this range by comparison with the calculated equilibration pressures of garnet-bearing xenoliths with similar temperatures (see below).

Geothermobarometry calculations for the four garnet-bearing granulites and the clinopyroxenite give 1.15–1.20 GPa at 800–900 °C (GM92-390 and GM92-165), 1.35 GPa at 800–900 °C (GM92-347) and 1.80 GPa at 925–1000 °C (GM92-394). These are within the experimentally determined 'garnet granulite stability field' (Irving 1974; Gasparik 1984).

Table 3 Electron microprobe analyses of minerals from Kerguelen Type II granulite and pyroxenite xenoliths (average values)

	Type IIa/IIc Cpx GM 92–394 $n=8$	Type IIa Cpx GM 92–347 $n=4$	Type IIa Cpx OB 93–57a $n=4$	Type IIa Cpx GM 92–412 $n=2$	Type IIb Cpx GM 92–165 $n=11$	Type IIc Cpx GM 92–390 $n=10$	Type IIa/IIc Opx GM 92–394 $n=6$	Type IIa Opx GM 92–347 $n=4$	Type IIa Opx OB 93–57a $n=3$	Type IIa Opx GM 92–412 $n=4$	Type IIb Opx GM 92–165 $n=2$	Type IIc Opx GM 92–390 $n=6$	Type IIa/IIc Plagioclase GM 92–394 $n=5$	Type IIa Plagioclase GM 92–347 $n=4$	Type IIa Plagioclase OB 93–57a $n=4$	Type IIa Plagioclase GM 92–412 $n=3$	Type IIb Plagioclase GM 92–165 $n=4$
SiO_2	50.7	51.7	49.2	51.0	48.9	49.4	53.8	55.1	51.0	51.2	52.4	52.2	57.5	49.4	50.1	47.0	58.8
TiO_2	1.20	0.20	0.79	0.19	1.20	0.80	0.20	–	0.12	0.04	0.20	0.10	0.03	0.01	0.04	0.02	0.03
Al_2O_3	7.80	7.10	6.65	7.35	7.80	6.90	3.50	4.60	5.20	7.89	3.60	3.00	26.34	31.54	31.07	33.06	25.18
Cr_2O_3	0.10	–	0.21	0.04	–	–	0.10	–	0.08	0.04	–	–	–	–	–	–	–
NiO	–	0.10	0.06	0.10	–	–	–	0.20	0.14	0.08	0.10	0.10	–	–	–	–	–
MgO	13.10	14.60	13.18	14.08	12.10	11.30	28.50	32.50	25.63	28.59	25.50	24.30	–	–	–	–	–
FeOt	5.20	3.00	6.42	4.59	7.60	9.00	12.70	7.50	15.54	11.05	16.90	18.60	0.13	0.10	0.14	0.15	0.28
MnO	0.10	–	0.12	0.13	0.10	0.10	0.10	–	0.29	0.19	0.30	0.30	0.01	0.02	0.03	–	–
CaO	19.80	22.30	21.60	21.67	20.00	19.80	0.90	0.50	0.60	0.76	1.00	0.70	8.81	15.14	14.07	16.62	7.24
Na_2O	1.90	1.10	1.04	0.97	1.60	1.90	0.10	0.10	0.09	0.08	0.10	0.10	6.68	2.99	3.61	2.21	7.27
K_2O	–	–	–	–	–	–	–	–	–	–	–	–	0.23	0.31	0.08	0.04	0.64
Total	99.9	100.1	99.6	100.2	99.7	99.7	100.0	100.7	98.9	100.2	100.2	99.4	99.8	99.6	99.1	99.1	99.6
mg#	81.79	89.66	78.54	84.54	73.94	69.12	80.00	88.54	74.62	82.18	72.90	69.96	–	–	–	–	–

	Type IIc Plagioclase GM 92–390 $n=7$	Type IIa/IIc Spinel GM 92–394 $n=3$	Type IIa Spinel GM 92–347 $n=3$	Type IIa Spinel OB 93–57a $n=3$	Type IIa Spinel GM 92–412 $n=3$	Type IIb Spinel GM 92–165 $n=3$	Type IIa/IIc Garnet GM 92–394 $n=5$	Type IIa Garnet GM 92–347 $n=2$	Type IIb Garnet GM 92–165 $n=3$	Type IIc Garnet GM 92–390 $n=4$	Type IIa Sapphirine GM 92–347 $n=3$	Type IIa Sapphirine GM 92–412 $n=3$	Type IIa/IIc Rutile GM 92–394 $n=4$	Type IIb Amphibole GM 92–165 $n=5$	Type IIc Amphibole GM 92–390 $n=2$	Type IIb Ilmenite GM 92–165 $n=2$	Type IIc Ilmenite GM 92–390 $n=3$
SiO_2	57.7	0.05	0.02	0.10	0.12	0.11	40.8	42.1	39.8	39.7	13.20	14.29	0.02	40.1	41.5	0.08	0.04
TiO_2	0.02	0.41	0.03	0.09	0.01	0.43	0.15	0.01	0.14	0.09	–	0.04	99.1	3.75	2.99	51.7	41.2
Al_2O_3	26.39	60.6	65.3	60.0	64.1	60.2	22.82	23.63	22.15	21.95	62.7	59.0	0.20	14.54	13.64	0.29	0.50
Cr_2O_3	–	2.11	0.96	0.28	0.93	0.33	0.07	0.06	0.01	0.02	0.50	0.37	0.10	0.05	0.09	0.02	0.13
NiO	–	0.38	1.01	0.31	0.31	0.11	0.02	–	–	0.02	0.40	0.11	–	0.04	0.03	0.04	0.02
MgO	–	16.49	20.35	15.52	18.70	16.08	15.59	19.51	11.99	11.17	18.90	18.58	–	11.67	12.17	4.44	2.88
FeO	0.21	18.13	10.58	22.65	14.53	21.45	14.77	9.57	18.37	20.28	4.10	6.79	0.30	12.24	12.55	41.33	50.99
MnO	0.01	0.07	0.02	0.15	0.09	0.14	0.37	0.14	0.81	0.91	–	0.04	–	0.15	0.06	0.78	0.39
CaO	8.70	–	–	0.06	–	–	5.43	5.49	6.69	5.83	–	0.07	–	10.54	10.49	0.24	0.09
Na_2O	6.79	–	–	–	–	–	–	–	–	–	–	0.03	–	3.15	3.56	–	–
K_2O	0.06	–	–	–	–	–	–	–	–	–	–	–	–	0.94	0.22	–	–
Total	100.0	98.5	98.4	99.8	99.0	99.4	100.1	100.7	100.2	100.1	99.80	99.38	99.72	97.2	97.3	99.4	98.4
mg#	–	61.8	77.4	55.0	69.6	57.2	65.3	78.4	53.8	49.5	89.2	83.0	–	63.0	63.3	–	–
cr#	–	2.28	0.98	0.31	0.96	0.37	–	–	–	–	–	–	–	–	–	–	–

Table 4 Calculated end member compositions for the constituent minerals of Type I harzburgite and Type II granulite and pyroxenite xenoliths

	Tholeiitic–transitional basalt affinity					Type IIb **GM92-165** Type II garnet pyroxenite Alkali basalt affinity	Type I **GM92-453** Type I harzburgite Peridotite mantle wall-rock
	Type II pyroxene granulites		Type II garnet two-pyroxene granulites				
	Type IIa **OB93-57a**	Type IIa **GM92-412**	Type IIa **GM92-347**	Type IIa/IIc **GM92-394**	Type IIc **GM92-390**		
Clinopyroxene	**40.50%**	**23%**	**25%**	**40%**	**46.50%**	**81.50%**	**2%**
CaTs	13.50	13.90	12.30	11.70	14.00	15.60	8.50
Ac	7.70	3.20	2.10	3.50	11.90	9.10	10.70
Jd	–	3.60	5.50	10.00	2.00	2.60	4.50
Di	67.83	69.16	73.73	63.51	57.03	59.43	67.16
Fs	10.97	10.14	6.37	11.29	15.07	13.27	9.14
Orthopyroxene	**18%**	**18%**	**2%**	**7.50%**	**1%**	**5.50%**	**13%**
CaTs	14.02	18.21	10.86	9.59	10.40	12.23	10.58
En	58.88	56.10	77.72	70.30	61.25	62.13	76.92
Fs	27.10	25.69	11.42	20.12	28.35	25.64	12.50
Plagioclase	**40%**	**49%**	**26%**	**27.50%**	**18%**	**3%**	
Xan	0.68	0.80	0.72	0.42	0.41	0.34	
Xab	0.32	0.20	0.26	0.57	0.58	0.62	
Xor	0.01	–	0.02	0.01	–	0.03	
Spinel	**1.50%**	**7%**	**2.50%**	**1.50%**	–	**4%**	**1%**
Hercynite	0.38	0.28	0.25	0.35		0.37	31.86
Pleonaste	0.62	0.72	0.75	0.65		0.63	21.98
Picochromite							27.14
Chromite							18.72
Garnet			**36%**	**23%**	**30%**	**1%**	
Xalm			0.18	0.28	0.40	0.36	
Xpyr			0.66	0.57	0.42	0.45	
Xgro			0.15	0.14	0.16	0.18	
Ilmenite				–	**4.50%**	**1.50%**	
Ilmenite				–	0.66	0.78	
Geikielite				–	0.08	0.18	
Hematite				–	0.26	0.04	
Olivine							**84%**
Fo							89.1
Fa							10.9
Other phases	**Sa: 3%**	–	**Sa: 8.5%**	**Ru: 0.5%**		**Am: 3.5%**	

Petrophysical characteristics

Measured density (ρ) and P-wave velocity (Vp)

Three orthogonal cores, 15–35 mm in length and 15 mm in diameter, were prepared from each of the selected xenoliths except sample GM92-165, which has only one core due to its small size. Most samples do not show shape preferred mineral orientation (SPO), but, where observed (sample GM92-412), the cores were cut parallel and orthogonal to it. The ends of the cores were ground flat and parallel within ± 0.01 mm. Densities were measured by immersion in ethanol. The significance of the measured densities depends upon the degree of interconnectivity of the network of cracks and pores. Isolated (i.e. non-interconnected) porosity within a specimen will be reflected in reduced bulk density, whereas a 'grain' density closely comparable with that calculated from the modal mineralogy (below) would be determined for a specimen with fully interconnected pore space.

The ultrasonic velocity measurements were performed in a Harwood pressure vessel at the petrophysics laboratory of the Research School of Earth Sciences, Australian National University. The vessel operates to 1 GPa confining pressure at room temperature. The cores (on which densities have been measured) were jacketed in copper sleeves sealed with O-rings against hardened steel end pieces in order to exclude the petroleum spirit pressure medium. After each successful run, the steel end pieces were removed and the sample examined to ensure that fluid had not penetrated into the pore space of the specimen. Detailed descriptions of the ultrasonic technique have been given by Jackson and Arculus (1984), O'Reilly et al. (1990) and Rudnick and Jackson (1995). Rock velocities were calculated from the zero-pressure core length and measured high-pressure travel time of the pulse. Estimated uncertainties of the measurements are 1% for compressional wave velocity and 0.01 g/cm^3 for density.

The experimental results of the measurements of the compressional wave velocities for each core of each

Table 5 Calculated pressures and temperatures of equilibration for Type II granulite and pyroxenite xenoliths from the Kerguelen Islands. In Brey and Kohler column (0.8 Gpa) is assumed P

		P (Gpa) Harley (1984)	T (°C) Wells (1977)	T (°C) Brey and Kohler (1990)	T (°C) Ellis and Green (1979)
Tholeiitic–transitional affinity					
Two-pyroxene granulites					
OB93-57a	Type IIa	–	862	800 (0.8)	–
GM92-412	Type IIa	–	900	890 (0.8)	–
Garnet two-pyroxene granulites					
GM92-347	Type IIa	1.35	865	800	850
GM92-394	Type IIa/IIc	1.80	925	930	1000
GM92-390	Type IIc	1.15	815	890	860
Alkali basalt affinity					
Garnet pyroxenite					
GM92-165	Type II	1.20	850	890	900
Mantle harzburgite					
GM92-453	Type I	–	–	1125	–

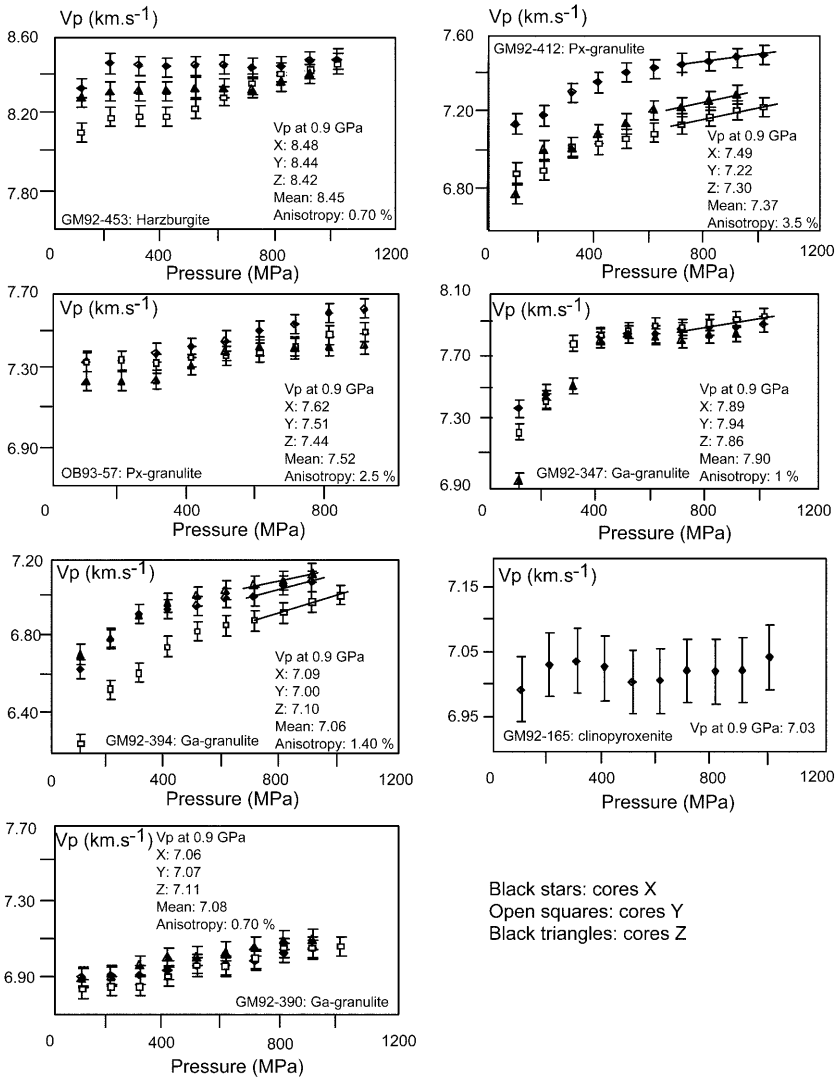

Fig. 6 Velocity vs. pressure for the three orthogonal cores (X, Y and Z) of Kerguelen granulite and pyroxenite xenoliths. For sample GM92-165 only one core was made because of the small size and disaggregated state of this rock

sample are shown as functions of pressure to 0.9 or 1 GPa in Fig. 6. The harzburgite (GM92-453) and the garnet clinopyroxenite (GM92-165) have higher densities (3.30 and 3.37 g/cm^3 respectively) than the mafic granulites, regardless of whether or not they contain garnet (3.04–3.25 g/cm^3).

Three granulites (GM92-412, GM92-347, GM92-394) show a marked increase in V_P with increasing P to

400 MPa (Fig. 6) – presumably reflecting the suppression of a substantial amount of crack porosity – with milder pressure sensitivity at higher pressures. This behaviour is typical of measurements on moderately coarse-grained rock specimens, especially xenoliths (e.g. O'Reilly et al. 1990; Rudnick and Jackson 1995). The densities (ρ) and the compressional (Vp) wave velocities measured at 0.9 GPa are tabulated in Table 6. Specimens GM92-453 and OB93-57 yield relatively high velocities at 0.9–1.0 GPa but without the much stronger pressure sensitivity at lower pressures – suggesting an unusual degree of mechanical competence in these specimens such that much of the crack porosity is closed at pressures lower than 100–200 MPa. Specimens GM92-165 and GM92-390 also display little pressure sensitivity, but at much lower velocities.

Comparison of the velocities measured on the orthogonal cores prepared from each xenolith reveals appreciable elastic anisotropy (i.e. $>1\%$) persisting to $\sim$1 GPa only for specimens GM92-394 (1.4%), OB93-57 (2.5%) and GM92-412 (3.5%). For this last specimen, a weak shape preferred orientation (SPO) is evident in hand specimen and thin section (see the petrographic description).

The two garnet-free pyroxene granulites (OB93-57 and GM92-412), both of tholeiitic–transitional geochemical affinity, have mean V_P at 0.9 GPa of 7.37 and 7.52 km/s respectively. The two garnet granulites GM92-390 and GM92-394 (also tholeiitic–transitional) have mean Vp of 7.08 and 7.06 km/s respectively. The more magnesian tholeiitic–transitional garnet-bearing granulite containing sapphirine (GM92-347) has the highest mean Vp of all the granulites (7.90 km/s at 0.9 GPa). The mantle harzburgite GM92-453 has a mean Vp of 8.45 km/s, the highest value for samples from Kerguelen studied here, as expected for its high *mg* number (89.93) and the high modal proportion of olivine (84%, Table 4).

Calculated density and P-wave velocities

Densities, elastic moduli and P-wave velocities for the xenoliths of this study have been calculated by the method of Jackson et al. (1990) using the modal proportions of the constituent minerals olivine, orthopyroxene, clinopyroxene, plagioclase, spinel, garnet and ilmenite, along with the appropriate single-crystal elasticity and density data from the literature (e.g. Table 7). The modes (Table 4) were calculated by a least-squares mixing program using the major element compositions of minerals and bulk rock composition. We did not include amphibole and sapphirine because amphibole has a very low modal abundance and there are no elasticity and density data for sapphirine. The modes used for calculations were adjusted for the removal of sapphirine.

The elastic moduli for mineral solid solutions are modelled as proportional molar averages of the end member properties (Table 4). This time-honoured approach has been documented previously (e.g. Leitner et al. 1980) and has recently been shown to reproduce accurately the measured elastic moduli for omphacitic pyroxene (Bhagat et al. 1992). Rarely, significant deviations from the molar average are observed and may be attributable to cation ordering effects (Bass and Weidner 1984).

The plagioclase and alkali feldspar end member properties of Jackson et al. (1990) are here replaced with those tabulated by Bass (1995) for albite, anorthite and microcline. We also add the properties for ilmenite given by Liebermann (1976) and Bass (1995). In addition there has been a dramatic expansion during the past two decades of the single-crystal elasticity data set for pyroxenes resulting from the use of opto-acoustic techniques on microcrystals (e.g. Kandelin and Weidner 1988; Chai et al. 1997). It is accordingly now feasible to model the elasticity of these phases much more realistically than has previously been attempted (e.g. Jackson et al. 1990). In particular, clinopyroxene elasticity data are now available not only for the quadrilateral end members (enstatite, ferrosilite, diopside and hedenbergite) but also for acmite, jadeite and Tschermak components.

The approach adopted here is to recalculate the analysed orthopyroxene compositions within the ternary system En–Fs–CaTs and the clinopyroxene com-

Table 6 Measured and calculated densities and seismic velocities (0.9 GPa) of the Type I and Type II Kerguelen xenoliths

	Density (g/cm^3) measured	Density (g/cm^3) calculated	Consistency (%)	Vp (km/s) measured (0.9 GPa)	Vp (kms) calculated	Consistency (%)
Harzburgite (peridotite mantle wall-rock)						
GM92-453	3.30	3.34	1	8.45	8.29	2
Pyroxene granulites (Type IIa): tholeiitic–transitional basaltic affinity						
GM92-412	3.06	3.09	1	7.37	7.43	1.5
OB93-57	3.08	3.13	1.5	7.52	7.39	2
Pyroxene garnet granulites (Type IIa, IIa/IIc and IIc): tholeiitic–transitional basaltic affinity						
GM92-347	3.25	3.32	2	7.9	7.99	1.5
GM92-394	3.04	3.27	7	7.06	7.69	8
GM92-390	3.17	3.48	9	7.08	7.78	9
Garnet pyroxenite (Type IIb): alkali basaltic affinity						
GM92-165	3.37	3.41	1	7.03	7.88	11

Table 7 Densities and elastic moduli for pyroxene end members. Unless otherwise indicated, densities are from Smyth and McCormick (1995) and elasticity data from Bass (1995)

Descriptor	Composition	Density (g/cm$^{3)}$	K (bulk modulus) (GPa)	G (shear modulus) (GPa)
Orthopyroxene				
Enstatite	$Mg_2Si_2O_6$	3.204	108	76
Ferrosilite	$Fe_2Si_2O_6$	4.002	101	52[a]
'Kilbourne Hole'[b]	$En_{80}Fs_9MgTs_7CaTs_4$	3.304	116	78
(Mg,Ca)Ts	$(Mg_{0.65}Ca_{0.35})AlAlSiO_6$	3.376[c]	183[d]	100[d]
Clinopyroxene				
Diopside	$CaMgSi_2O_6$	3.279	113	67
Hedenbergite	$CaFeSi_2O_6$	3.656	120	61
Jadeite	$NaAlSi_2O_6$	3.341	143	85
Acmite	$NaFeSi_2O_6$	3.576	112	59
CaTs	$CaAlAlSiO_6$	3.438	143[e]	85[e]

[a]Molar averages based on G = 72 GPa provide a better fit to the moduli measured on solid solutions of bronzite composition
[b]Chai et al. (1997)
[c]Estimated from data tabulated for clinoenstatite, diopside and CaTs by Smyth and McCormick (1995)
[d]Required to reconcile data for the Kilbourne Hole aluminous orthopyroxene (Chai et al. 1997) with the molar average of end member moduli
[e]As for jadeite (see text)

positions as a combination of the five end members Di, Hd, Ac, Jd and CaTs. This approximation to the measured compositions of the generally aluminous pyroxenes consistently accounts for more than 95% of the analysis. The bulk and shear moduli of each of these end member phases appropriate for elastically isotropic polycrystals as calculated or inferred from single-crystal elasticity measurements are presented in Table 7.

The substantially higher bulk and shear moduli for jadeite than for Al-free pyroxenes are attributed mainly to the stiffening of the Al-accommodating M1 octahedral site (Kandelin and Weidner 1988). Significantly, this feature of the jadeite structure is partly shared by CaTs in which Al is distributed between the M1 octahedral and the tetrahedral sites. Na in jadeite is replaced by Ca in the M2 sites of CaTs, and half of the Si in jadeite is replaced by Al in the tetrahedral sites of CaTs. The $(Ca/Na)^{M2}$ and $(Al/Si)^{T}$ substitutions may be expected to have opposing influences upon the elastic moduli that will tend to cancel. Accordingly, the elastic moduli of CaTs can reasonably be approximated by those for jadeite (Table 7). For MgTs, the substitution $(Mg/Ca)^{M2}$ is expected to result in moduli substantially higher even than for CaTs and jadeite, in accord with the inferences drawn from the properties of the Kilbourne Hole orthopyroxene (Table 7).

The correlation between the measured densities and mean (0.9–1.0 GPa) compressional wave velocities and the primary mineralogy of the xenoliths has been assessed by comparison with the corresponding properties calculated from the modal mineralogy (Table 4) and appropriate density and single-crystal elasticity data (as described above in the Methods section).

The calculated densities and P-wave velocities (Fig. 7; Table 6) are in good agreement (within 1–2 and 1.5–2% respectively) with their measured equivalents for four samples (harzburgite GM92-453, the pyroxene-granulites GM92 412 and OB93-57, and one of the three garnet granulites GM92-347). The other two garnet granulites (GM92-394 and GM92-390) give substantially lower measured V_P and densities than are calculated from the modal mineralogy (Table 3). Garnet clinopyroxenite (GM92-165) has similar calculated and measured densities but lower measured than calculated P-wave velocity (Fig. 7).

There are several possible explanations for discrepancies commonly observed between the P-wave velocities measured on xenoliths and those calculated from the modal mineralogy as discussed by Rudnick and Jackson (1995) for mafic granulite xenoliths from the Chudleigh volcanic province (North Queensland, Australia). Scattering of elastic waves at grain boundaries is not applicable to the Kerguelen xenoliths for the same reasons given by Rudnick and Jackson (1995). Neither are compositional effects due to the pyroxenes relevant because we have accounted in this study for the Al and Na

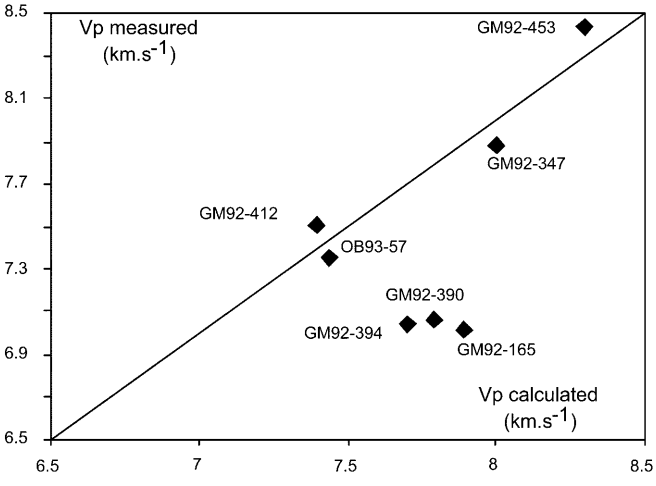

Fig. 7 Measured velocity (0.9 GPa) plotted against calculated velocity (mean values) of Kerguelen granulite and pyroxenite xenoliths

contents of the pyroxenes. Our method of calculation of the modal composition of the samples is based on representative bulk rock and mineral analyses and is unlikely to be a source of significant error. It is also unlikely that there is an error in the modal composition for only three samples that moreover produces a systematic shift to higher values for the velocities calculated for these samples.

Two likely possibilities therefore remain to explain the observed discrepancy between measured and calculated Vp: grain boundary alteration in some xenoliths and/or failure to close all cracks and pore spaces at 0.9 GPa.

Petrographic studies of the Kerguelen xenoliths have shown that one feature common to samples GM92-390 and GM92-394 is the partial but significant replacement of garnet with kelyphite (from 20 to 80%). Those kelyphites are a secondary alteration product of lower density ($\sim$3.3 versus $\sim$3.8 g/cm^3) and compressional wave speed (8.0 versus 8.8–8.9 km/s), resulting from breakdown of the garnet due to decompression (Rudnick and Jackson 1995) or heating (e.g. Griffin et al. 1984, 1987). The measured densities and wave speeds of the two xenoliths GM92-390 and GM92-394 are lower than the calculated ones and could be explained by significant conversion of garnet to kelyphite; this suggests the presence of porosity that is not interconnected, presumably associated with the transformation of garnet to kelyphite. The coarse-grained garnet clinopyroxenite GM92-165 is pervasively fractured and shows clear evidence of grain-boundary alteration. Interconnectivity of the fracture network resulting in the measurement of a grain density would explain the approximate consistency between measured and calculated densities for this specimen. The low and pressure-insensitive wave speeds suggest that pressure is ineffective in closing the grain-boundary porosity in this specimen.

In view of the discrepancies between measured and calculated wave speeds for three of the seven xenoliths, the wave speeds calculated for the seven studied Kerguelen samples, suitably corrected to in situ P–T conditions, provide the more robust basis for the following discussion.

Discussion

Origin of the xenoliths:

Based on their petrographic, major element and REE characteristics, Grégoire et al. (1998) have proposed that the Type II Kerguelen xenoliths are either deep basaltic cumulates of the tholeiitic–transitional (Type IIa) or alkaline (Type IIb) magmatic series of the archipelago or else deep frozen tholeiitic–transitional basaltic melts (Type IIc). The major and trace element features of the studied Type II xenoliths in this paper emphasise these origins and highlight some new characteristics.

Kempton and Harmon (1992) showed that the relationship between mg number and SiO_2/Al_2O_3 can be used to identify granulites that had formed by accumulation of specific mineral phases from those representing solidified melts (Fig. 3). The Type IIa, IIa/IIc and IIb xenoliths lie near or in the Mafic 1 field in this plot, indicating that they are cumulates of original plagioclase and pyroxene (or olivine). The Type IIc xenolith plots in the 'primitive' basaltic magma field, indicating that the Type IIc xenoliths represent frozen basaltic melts. The petrological and geochemical characteristics of sample GM92-394 are intermediate between those of the Type IIa and Type IIc xenoliths and indicate that a compositional continuum exists between the deep tholeiitic–transitional cumulates and frozen melts.

Significance of petrophysical data and comparison with the seismic data and models

The V_P data derived in this study, along with the geochemical and geothermobarometry data from the same xenoliths, allow a re-interpretation of existing seismic data (Recq et al. 1990, 1994; Charvis et al. 1995) and the construction of likely rock-type sections for the crust–mantle boundary and the lithospheric mantle column (i.e. below the oceanic layer 3) beneath the Kerguelen archipelago.

Geothermobarometry calculations of this study show that the studied Type II xenoliths are derived from the depth range of about 35 to 55 km beneath the Kerguelen Islands (corresponding to the calculated pressure range of about 1.1 to 1.8 GPa). The associated equilibrium temperatures inferred from the primary mineralogy of the granulites and pyroxenite vary between about 800 and 1000 °C. It is important to note that granulites may occur intercalated with peridotites in the upper mantle (e.g. Pearson and O'Reilly 1991; Pearson et al. 1991 and references therein) and do not exclusively signify crustal facies. The Type I (harzburgite) xenolith (mantle wall-rock) has an equilibration temperature of 1125 °C (using the two-pyroxene thermometer of Brey and Kohler 1990 in Grégoire et al. 2000) and thus is derived from a level deeper than the Type II xenoliths. The transitional zone, which is about 3 km thick, has relatively low velocity, and is interpreted as representing the crust–mantle boundary from the seismic data (Recq et al. 1990). It lies below oceanic layer 3 (shown between 18 to 21 km in Fig. 8). Therefore, no xenoliths within the extensive suite studied so far (e.g. Grégoire et al. 1994, 1998) provide samples of the lithospheric column shallower than about 30–35 km. The mantle sample provided by xenoliths is always plagued by the capricious entrainment characteristics of the host magmas (e.g. O'Reilly 1989). However, Grégoire et al. (1998) have been able to recognise the different xenolith types evidencing multiple events of magmatic intrusion in the mantle beneath Kerguelen that correlate well with the tectonic and magmatic history of the region. We are therefore confident that the

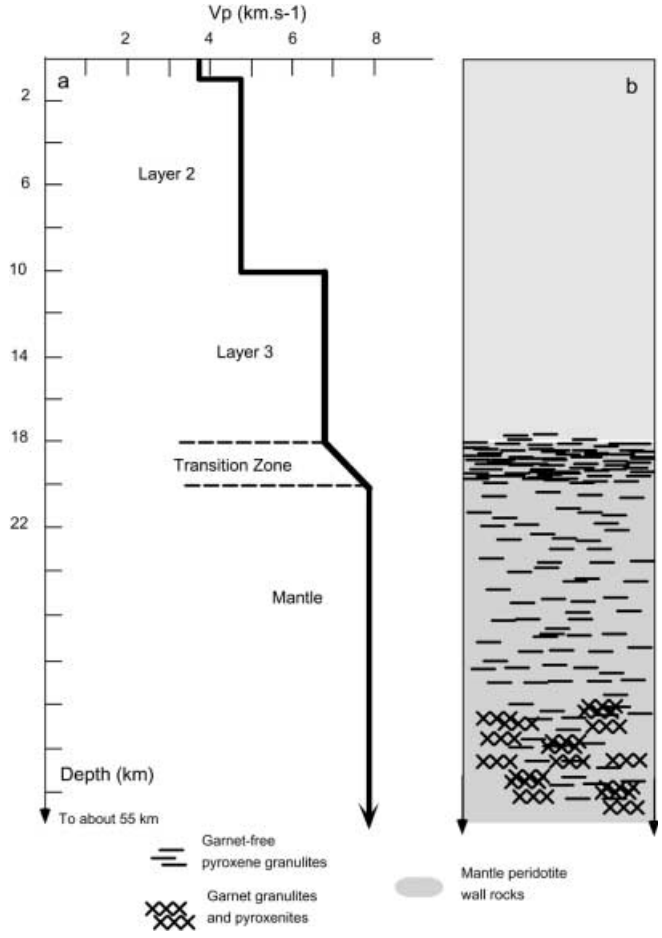

Fig. 8 **a** Vp–depth models for the Kerguelen Islands (after Recq et al. 1990, 1994). **b** Model for crust–mantle boundary (CMB) beneath the Kerguelen Islands. The 2–3 km transitional zone below oceanic layer 3 of the Kerguelen plateau is best explained by a varying mixture of pyroxene granulites and ultramafics with the proportion of the latter material increasing downwards. Lateral heterogeneities seen seismically in the Kerguelen upper mantle and the low average wave speeds can be explained by variable proportions of the garnet granulites and pyroxenites and harzburgite rock types characterised in this study, along with an anomalously high average temperature. Such lithological heterogeneity results from intrusions of basaltic magmas into the mantle wall-rock, consistent with other evidence of sustained voluminous magmatic activity in this region

xenolith suite available represents the deep-seated rock-type variability within this lithospheric column and can be used to infer the rock-type mix at shallower levels between about 55 km and oceanic layer 3.

The compressional wave speeds calculated (and in favourable circumstances measured) for the xenoliths of the Kerguelen suite indicate V_P is ~7.4 km/s for the pyroxene granulites and 7.7–8.0 km/s for the garnet granulites and pyroxenite respectively. These values compare with the ranges of measured (600 MPa) V_P for garnet-free (6.79–7.45 km/s) and garnet-bearing (7.03–7.50 km/s) mafic granulites from various localities given by Rudnick and Fountain (1995). The garnet-free Kerguelen granulites thus have calculated (and measured) wave speeds as high as any previously reported for pyroxene granulites, and the garnet granulites from Kerguelen are distinctly higher in wave speed than those from other localities. The high wave speeds are attributable to the distinctive major element compositions of these Kerguelen xenoliths. The cumulates that dominate this granulite suite are highly magnesian [100 Mg/(Mg + Fe) = 75–82] and also very aluminous (up to 23 and 26 wt% Al_2O_3 for GM92-347 and GM92-412). These compositional characteristics are reflected in the aluminous compositions of the pyroxenes and the relatively large amounts of modal garnet in the garnet granulites. These factors combine to explain the unusually high wave speeds calculated (and measured) for the Kerguelen granulite suite. The calculated and (1 GPa) measured wave speeds for the harzburgite GM92-453 and the calculated wave speed for the pyroxenite GM92-165 are unexceptional and fall within the field identified by O'Reilly et al. (1990) and Rudnick and Fountain (1995) for ultramafic rocks.

For meaningful comparison with seismic wave speeds for the deep crust and upper mantle beneath Kerguelen, the calculated (or measured) V_P need to be adjusted for in situ conditions of pressure and temperature. The appropriate temperature and pressure derivatives, determined in high-frequency ultrasonic studies, are $\partial Vp/\partial T = -5 \times 10^{-4}$km/s/K and $\partial Vp/\partial P =$ 0.1km/s/Gpa (e.g. Jackson 1991). The additional effect of viscoelastic relaxation (Minster and Anderson 1981, equation 43) is negligible (< 0.05 km/s) for relatively short-period P-waves under conditions appropriate to the upper mantle beneath Kerguelen.

The granulites and pyroxenites are interpreted as magmatic intrusions underplated and/or intruded around the crust–mantle boundary and intercalated throughout the lithospheric mantle (represented by the harzburgite) analogous to many continental lithospheric sections (e.g. O'Reilly and Griffin 1987; Deemer and Hurich 1994) and other oceanic regions where there has been significant volcanic activity (e.g. Agulhas: Uenzelmann-Neben et al. 1999; Gohl and Uenzelmann-Neben 2001; Iceland: Operto 1995; Marquesas: Caress et al. 1992).

The V_P values calculated for these xenoliths, suitably adjusted to in situ pressures and temperatures, are 7.1 km/s for the pyroxene granulites, 7.4–7.7 km/s for the garnet granulites and pyroxenite, and 8.0 km/s for the harzburgite. It follows that the transitional layer (V_P~7.2–7.5 km/s at depths of 18–21 km) beneath layer 3 of the oceanic crust is most plausibly interpreted as an interlayering of pyroxene granulites and ultramafic rocks with increasing proportions of mantle wall-rock with increasing depth through the transition zone (Fig. 8). As garnet is not stable in granulite compositions at this relatively shallow depth, the garnet granulites would not contribute to this part of the lithospheric column: they become stable at a depth of about 30 km (Grégoire et al. 1994, 1998). A similar mixture of rock types has been well-constrained for some continental regions with more continuous xeno-

lith sampling of the relevant depth range (e.g. O'Reilly and Griffin 1987).

The seismic data reveal two other characteristics of the mantle beneath the Kerguelen plateau (Recq et al. 1990): lateral variations of the velocity gradient within the upper mantle and relatively low P-wave velocities (7.7–7.95 km/s) for the upper mantle. These observations might be explained by variable proportions of mafic (garnet granulites and pyroxenites) and ultramafic (harzburgite) lithologies within the upper mantle. This is consistent with the indications from the geothermobarometry that the mafic rock types are present to depths of at least 55 km and therefore are mixed with the mantle wall-rocks. The generally low and spatially variable wave speeds are probably also indicative of a broad thermal anomaly. For a given lithology, the sensitivity of V_P to temperature variation should be ~–0.1 km/s per 200 °C.

The mantle harzburgite of this study has a calculated density of 3.34 g/cm^3 (the measured value is even lower at 3.30 g/cm^3), which is significantly less dense than young subcontinental mantle (3.37 g/cm^3) or primitive mantle (3.39 g/cm^3). It is similar to relatively buoyant Proterozoic mantle (3.34 g/cm^3), as documented in Griffin et al. (1999), but has a higher density than depleted very buoyant Archean mantle (3.31 g/cm^3) because of its higher Fe content. In addition, the densities of the pyroxenites and garnet granulites range to values (3.27 g/cm^3) significantly lower than the harzburgite density. These results are consistent with those of Charvis et al. (1995) and those inferred from the geoid data by Marks and Sandwell (1991), indicating the occurrence of relatively low-density material to about 80 km deep in the mantle beneath Kerguelen in order to achieve the local isostatic compensation.

Conclusions

Measured and calculated values of V_P for rock samples representative of the crust–mantle boundary and upper mantle beneath the Kerguelen plateau define three ranges: ~7.4 km/s for pyroxene granulites, 7.7 to 8.0 km/s for garnet granulites and 8.3 km/s for harzburgite (peridotite mantle wall-rock). Measured and calculated values of V_P are in good agreement for samples free of kelyphitic transformation of garnet and grain-boundary alteration. These wave speeds need to be adjusted downward by 0.3–0.4 km/s for in situ conditions (1–2 GPa, 800–1100 °C) determined through geothermobarometry.

The 2–3 km transitional zone from about 18 to 20 km below oceanic layer 3 of the Kerguelen plateau is best explained by a varying mixture of pyroxene granulites and ultramafics with the proportion of the latter material increasing downwards. Lateral heterogeneities seen seismically in the Kerguelen upper mantle and the low average wave speeds (Recq et al. 1990, 1994; Charvis et al. 1995) can be explained by variable proportions of the garnet granulites and pyroxenites and harzburgite rock types characterised in this study, along with an anomalously high average temperature. Such lithological heterogeneity results from intrusions of basaltic magmas into the mantle wall-rock, consistent with other evidence of sustained voluminous magmatic activity in this region (Gautier et al. 1990; Giret 1993; Weis et al. 1993; Grégoire et al. 1998).

The relatively low density of the Kerguelen mantle to about 80 km is also consistent with the relatively low density of the depleted mantle and the intercalated basaltic rock types equilibrated to mantle conditions.

Acknowledgements This work has been made possible by the generous assistance and technical expertise of N.J. Pearson, A. Sharma, C. Lawson (GEMOC Geochemical Analysis Unit) H. Kokkonen and R. Guziak (Petrophysic laboratory, RSES, ANU). This work has been supported by a Macquarie University Research Fellowship and Grant Schemes (M.G.), Australian Research Council Large and Small Grants (S.Y. O'R., M.G.) and CNRS and IFRTP grants (J-Y. C.). We appreciate the continuing advice and input of A. Giret. We also thank the French Polar Research and Technology Institute (IFRTP, Brest, France) and the University Jean Monnet (St. Etienne, France) for their support. D. Smith, H. Kern, K. Mengel, J. Hoefs and an anonymous reviewer are gratefully acknowledged for providing constructive and thorough reviews. This is Publication 244 of the ARC National Key Centre for the Geochemical Evolution and Metallogeny of Continents (www.es.mq.edu.au/GEMOC/).

References

Bass JD (1995) Elasticity of minerals, glasses and melts. In: Ahrens TJ (ed) Mineral physics and crystallography: a handbook of physical constants. Am Geophys Union, Washington, pp 45–63

Bass JD, Weidner DJ (1984) Elasticity of single-crystal orthoferrosilite. J Geophys Res 89:4359–4371

Bhagat SS, Bass JD, Smyth JR (1992) Single-crystal elastic properties of omphacite-C2/c by Brillouin spectroscopy. J Geophys Res 97:6843–6848

Brey GP, Köhler T (1990) Geothermometry in four-phase lherzolites. II. New thermobarometers, and practical assessment of existing thermobarometers. J Petrol 31:1353–1378

Caress DW, Mutter JC, McNutt MK, Detrick RS (1992) An OBS refraction experiment across the Marquesas islands: the deep crustal structure of a hot-spot trace. EOS Trans Am Geophys Union 73:489–490

Chai M, Brown JM, Slutsky LJ (1997) The elastic constants of an aluminous orthopyroxene to 12.5 GPa. J Geophys Res 102:14779–14785

Charvis P, Recq M, Operto S, Brefort D (1995) Deep structure of the northern Kerguelen plateau and hotspot-related activity. Geophys J Int 122:899–924

Coffin MF, Eldhom O (1993) Scratching the surface: estimating dimensions of large igneous provinces. Geology 21:515–518

Coisy P, Nicolas A (1978) Structure et géodynamique du manteau supérieur sous le Massif Central (France) d'après l'étude des enclaves des basaltes. Bull Mineral 4:424–436

Deemer SJ, Hurich CA (1994) The reflectivity of magmatic underplating using the layered mafic intrusion analog. Tectonophysics 232:239–255

Ellis DJ, Green DH (1979) An experimental study of the effect of Ca upon garnet–clinopyroxene Fe–Mg exchange equilibria. Contrib Mineral Petrol 71:13–22

Finlayson DM, Leven JH (1987) Lithospheric structures and possible processes in eastern Australia from deep seismic investigations. Tectonophysics 133:199–215

Frey FA, Prinz M (1978) Ultramafic inclusions from San Carlos, Arizona. Petrologic and geochemical data bearing on their petrogenesis. Earth Planet Sci Lett 38:139–176

Gasparik T (1984) Two-pyroxene thermobarometry with new experimental data in the system CaO–MgO–Al_2O_3–SiO_2. Contrib Mineral Petrol 87:87–97

Gautier I, Weis D, Mennessier JP, Vidal P, Giret A, Loubet M (1990) Petrology and geochemistry of the Kerguelen Archipelago basalts (South Indian Ocean): evolution of the mantle sources from ridge to intraplate position. Earth Planet Sci Lett 100:59–76

Giret A (1993) Les étapes magmatiques de l'édification des îles Kerguelen. Bull Soc Geol Fr/Bull APBG, Spec Issue, pp 273–282

Giret A, Grégoire M, Cottin JY, Michon G (1997) The Kerguelen islands: the third type of oceanic islands. In: Ricci CA (ed) The Antarctic region: geological evolution and processes. Terra Antarctica Publication, pp 735–741

Gohl K, Uenzelmann-Neben G (2001) The crustal role of the Agulhas Plateau, southwest Indian Ocean: evidence from seismic profiling. Geophys J Int 144:632–646

Grégoire M, Mattielli N, Nicollet C, Cottin JY, Leyrit H, Weis D, Shimizu N, Giret A (1994) Oceanic mafic granulite from the Kerguelen Archipelago. Nature 367:360–363

Grégoire M, Cottin JY, Mattielli N, Nicollet C, Weis D, Giret A (1995) The Kerguelen archipelago: an hypothetic continental mafic protolith. Terra Antarctica 2(1):1–6

Grégoire M, Lorand JP, Cottin JY, Giret A, Mattielli N, Weis D (1997) Petrology of Kerguelen mantle xenoliths: evidence of a refractory oceanic mantle percolated by basaltic melts beneath the Kerguelen archipelago. Eur J Mineral 9:1085–1100

Grégoire M, Cottin JY, Giret A, Mattielli N, Weis D (1998) The metaigneous xenoliths from Kerguelen archipelago: evidence of a continent nucleation in an oceanic setting. Contrib Mineral Petrol 133:259–283

Grégoire M, Moine BN, O'Reilly SY, Cottin JY, Giret A (2000) Trace element residence and partitioning in mantle xenoliths metasomatised by high alkaline silicate- and carbonate-rich melts (Kerguelen Islands, Indian Ocean). J Petrol 41:477–509

Griffin WL, Wass SY, Hollis JD (1984) Ultramafic xenoliths from Bullenmeri and Gnotuk maars, Victoria, Australia: petrology of a subcontinental crust–mantle boundary. J Petrol 25:53–87

Griffin WL, Sutherland FL, Hollis JD (1987) Geothermal profile and crust–mantle transition beneath east-central Queensland: volcanology, xenolith petrology and seismic data. J Volcanol Geotherm Res 31:177–203

Griffin WL, O'Reilly SY, Ryan CG (1999) The composition and origin of sub-continental lithospheric mantle. In: Fei Y, Bertka CM, Mysen BO (eds) Mantle petrology: field observations and high-pressure experimentation. A tribute to Francis R. (Joe) Boyd, Geochemical Society, Spec Pub No 6, pp 13–43

Harley SL (1984) The solubility of alumina in orthopyroxene coexisting with garnet in FeO–MgO–Al_2O_3–SiO_2 and CaO–FeO–MgO–Al_2O_3–SiO_2. J Petrol 25:665–696

Irving AJ (1974) Geochemical and high pressure experimental studies for garnet pyroxenite and pyroxene granulite xenoliths from the Delegate basaltic pipe, Australia. J Petrol 15:1–40

Jackson I (1991) The petrophysical basis for the interpretation of seismological models for the continental lithosphere. In: Drummond BJ (ed) The Australian lithosphere. Geol Soc Aust Spec Publ 17, pp 81–114

Jackson I, Arculus RJ (1984) Laboratory wave velocity measurements on lower crustal xenoliths from Calcutteroo, South Australia. Tectonophysics 101:185–197

Jackson I, Rudnick RL, O'Reilly SY, Bezant C (1990) Measured and calculated elastic wave velocities for xenoliths from the lower crust and upper mantle. Tectonophysics 173:207–210

Kandelin J, Weidner DJ (1988) The single-crystal elastic properties of jadeite. Phys Earth Planet Inter 50:251–260

Kempton PD, Harmon RS (1992) Oxygen isotope evidence for large-scale hybridization of the lower crust during magmatic underplating. Geochim Cosmochim Acta 56:971–986

Leitner BJ, Weidner DJ, Liebermann RC (1980) Elastic of single crystal pyrope and implications for garnet solid solution series. Phys Earth Planet Inter 22:111–121

Liebermann RC (1976) Elasticity of ilmenites. Phys Earth Planet Inter 12:5–10

Marks KM, Sandwell DT (1991) Analysis of geoid height versus topography for oceanic plateaux and swells using nonbiased linear regression. J Geophys Res 96:8045–8055

McDonough WF, Sun S (1995) The composition of the Earth. Chem Geol 120:223–253

Minster JB, Anderson DL (1981) A model of dislocation-controlled rheology for the mantle. Philos Trans R Soc Lond 299:319–356

Operto S (1995) Structure et origine du Plateau de Kerguelen (Ocean Indien Austral): implications geodynamiques. These d'Universite, Univ Paris VI

O'Reilly SY (1989) Australian xenolith types, distribution and transport. In: Johnson RW (ed) Intraplate volcanism in eastern Australia and New Zealand. Cambridge University Press, Cambridge, pp 249–253

O'Reilly SY, Griffin WL (1987) Eastern Australia – 4000 kilometers of mantle samples. In: Nixon PH (ed) Mantle xenoliths. Wiley, Chichester, pp 267–280

O'Reilly SY, Griffin WL (1988) Mantle metasomatism beneath western Victoria, Australia, I: Metasomatic processes in Cr-diopside lherzolites. Geochim Cosmochim Acta 52:433–447

O'Reilly SY, Jackson I, Bezant C (1990) Equilibration temperatures and elastic wave velocities for upper mantle rocks from eastern Australia: implications for the interpretation of seismological models. Tectonophysics 185:67–82

Pearson NJ, O'Reilly SY (1991) Thermobarometry and P–T–t paths: the granulite to eclogite transition. J Metamorph Geol 9:349–359

Pearson NJ, O'Reilly SY, Griffin WL (1991) The granulite to eclogite transition beneath the eastern margin of the Australian craton. Eur J Mineral 3:293–322

Recq M, Brefort D, Malod J, Veinante JL (1990) The Kerguelen Isles (southern Indian Ocean): new results on deep structure from refraction profiles. Tectonophysics 182:227–248

Recq M, Le Roy I, Charvis P, Goslin J, Brefort D (1994) Structure profonde du mont Ross d'après la sismique (îles Kerguelen, océan Indien austral). Can J Earth Sci 31:1806–1821

Rudnick RL, Fountain DM (1995) Nature and composition of the continental crust: a lower crustal perspective. Rev Geophys 33:267–310

Rudnick RL, Jackson I (1995) Measured and calculated elastic wave speeds in partially equilibrated mafic granulite xenoliths: implications for the properties of an underplated lower continental crust. J Geophys Res 100:10211–10218

Smyth JR, McCormick TC (1995) Crystallographic data for minerals. In: Ahrens TJ (ed) Mineral physics and crystallography: a handbook of physical constants. Am Geophys Union, Washington, pp 45–63

Uenzelmann-Neben G, Gohl K, Ehrhardt A, Seargent M (1999) Agulhas Plateau, SW Indian Ocean: new evidence for excessive volcanism. Geophys Res Lett 26:1941–1944

Weis D, Frey FA, Leyrit H, Gautier I (1993) Kerguelen Archipelago revisited: geochemical and isotopic study of the S.E. Province lavas. Earth Planet Sci Lett 118:101–119

Wells PRA (1977) Pyroxene thermometry in simple and complex systems. Contrib Mineral Petrol 62:129–139

Wood BJ, Holloway JR (1984) A thermodynamic model for subsolidus equilibria in the system CaO–MgO–Al_2O_3–SiO_2. Geochim Cosmochim Acta 48:159–176

Xu X, O'Reilly SY, Griffin WL (1998) The geotherm of the lithosphere beneath Qilin, SE China: a reappraisal and implications for P–T estimation of Fe-rich pyroxenites. Lithos 47:115–119

Yang H-Y, Frey FA, Weis D, Giret A, Pyle D, Michon G (1998) Petrogenesis of the flood basalts forming the Northern Kerguelen Archipelago: implications for the Kerguelen Plume. J Petrol 39:711–748